0273-2289/02/98-100/1187/$15.00

Molecular Distillation

Rigorous Modeling and Simulation for Recovering Vitamin E from Vegetal Oils

C. B. Batistella, E. B. Moraes, R. Maciel Filho, and M. R. Wolf Maciel*

Separation Process Development Laboratory (LDPS). Faculty of Chemical Engineering, State University of Campinas, (UNICAMP), CP 6066, 13081-970, Campinas-SP, Brazil. E-mails: cesarb@ncap.com.br and wolf@feq.unicamp.br

Abstract

In this work, important results from simulations are presented, showing the potentiality of the molecular distillation process for recovering vitamin E from vegetal oils. Two types of molecular distillators are considered: falling film and centrifugal. The results emphasize the degree of recovery and factors that influence substantially the performance of the molecular distillators, such as feed flow rate, residence time, and process temperature. Moreover, they show that each type of molecular distillator enables one to operate under specific residence time and temperature. Therefore, a careful analysis must be made in order to determine the best equipment and operating conditions for obtaining products with high quality and concentration, and reduced problems of material thermal decomposition. Vitamin E (tocopherols) from vegetal oils, more specifically, from the deodorizer distillate of soya oil, was the studied case.

Index Entries: Molecular distillation; vegetal oils; vitamin E; soya oil.

Introduction

The substitution of conventional materials used in the nutrition, pharmaceutical, and cosmetic areas by natural products has gained interest and importance. An example is the product derived from refined vegetable oils, as the deodorizer distillate of vegetable oils (DDVO); palm oil for obtaining provitamin A *(1,2)*, oils of rice for the oryzanol recovery *(3)*, among others, can also be cited.

*Author to whom all correspondence and reprint requests should be addressed.

Molecular distillation is a peculiar case of evaporation, which happens in extremely low pressures and, therefore, in low temperatures *(4)*. Another important characteristic of molecular distillation is the reduced time in which the material is submitted to the process temperature, usually from 1 s to 1 min. This reduces, considerably, the effects of thermal decomposition. In a general way, these peculiarities show the high potential of this process in the separation, purification, and/or concentration of natural products, usually constituted by complex and thermally sensitive molecules *(1)*. Furthermore, this process can take advantage of other techniques that use solvents as the separating agent, avoiding problems with toxicity.

Taking all of this into consideration, in this work, the molecular distillation process for recovering tocopherols (for obtaining vitamin E), using the deodorizer distillate of soya oil (DDSO) with the conditions and the quality demanded by the market, is being proposed.

Molecular distillation is a process that requires a great deal of knowledge of its performance before it can be carried out. Small variations in the process conditions can lead to considerable alterations in the characteristics of the product streams. Therefore, it is very important to have simulation results first, to guide the experimental work *(5)*. Modeling and simulations of the process were then developed for recovering tocopherols (vitamin E) from DDSO, in order to determine the feasibility of the process and the best experimental conditions.

Tocopherols are a mixture of α-, β-, γ-, δ-tocopherols, which can be found in several proportions and concentrations, and they are present in vegetable oils such as soy, sunflower, canola, cotton, corn, palm, and rice *(6)*. They are particularly present in large amounts in the deodorizer distillate of soya oil (by product of the production of the vegetable oil) *(7)*. The deodorizer distillate is composed, basically, of fatty acids, triglycerides, diglycerides, monoglycerides, hydrocarbon, terpenols, and other materials, besides tocopherols and fitosterols.

Liquid Phase Mathematical Modeling

The mathematical modeling of molecular distillation is developed in two parts: first, the equations governing the liquid phase are considered, and, then the equations representing the vapor phase. The final modeling considering both phases permits through simulation the determination of important variables representing the system in study throughout the process.

Falling Film Equipment

A typical apparatus for the falling film molecular distillation is shown in Fig. 1. The materials flow throughout the equipment and the geometric coordinates are shown schematically in Fig. 2 *(8)*. The main part of the installation consists of a cylindrical evaporator surrounded by a condenser jacket. The liquid to be distilled is transported from a storage tank through

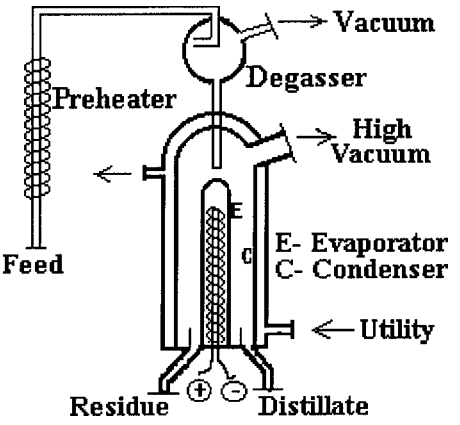

Fig. 1. Falling film molecular distillator.

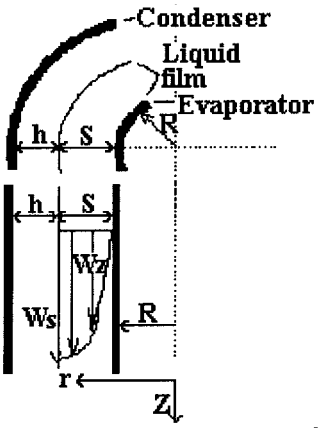

Fig. 2. The coordinate system and velocity distribution for the falling film.

a preheater to the surface of the unheated evaporator. It is also possible to heat the evaporator internally. In the case of a heated evaporator, the distillation rate is faster, but the separation factor decreases at higher temperatures. Figure 2 presents the velocity distribution in a film flowing down the evaporator.

Surface Evaporation Rate (High Vacuum)

The rate of surface evaporation, E_i (kg/m^{2}s), is obtained from the kinetic theory of gases, taking into account the anisotropic properties of the vapor [number of collisions is too low *(9)*]. Then, the evaporating rate equation is given by *(8)*:

$$E_i = C_{iS} P_i^{\text{sat}} \left(\frac{M_i}{2\pi R_g T_S} \right)^{\frac{1}{2}} \left[1 - (1 - F)\left(1 - e^{-\frac{h}{k\beta}}\right)^n \right] \quad (1)$$

where C_{iS} is the mole fraction in the liquid surface, P_i^{sat} is the vapor pressure (Pa), M_i is the molecular weight (g/gmol), R_g is the gas constant (J/kmol·K), T_S is the surface temperature of the liquid phase (K), and F, n, k, h, and β are constants, given by *(8)*.

Velocity and Thickness Profiles

The velocity is the one corresponding to a laminar and isothermal film with a smooth surface. Under such conditions, the velocity profile in the film is given by *(8)*:

$$W_Z = \frac{g\rho}{\eta} S^2 \left[\frac{r-R}{S} - \frac{1}{2}\left(\frac{r-R}{S}\right)^2 \right] \tag{2}$$

where W_z is the axial velocity (m/s), ρ is the mean liquid density (kg/m^3), η is the viscosity (Pa·s), and S is the thickness of the liquid film on the evaporator.

The feed flow rate and the continuity equations for the evaporating film give the film thickness:

$$S = \left[3\eta \left(\frac{m_0}{2\pi R g \rho^2} - \frac{1}{g\rho^2} \int_{z_0}^{z} (\Sigma E_i)\, dz \right) \right]^{\frac{1}{3}} \tag{3}$$

where S is the film thickness (m), m_0 is the feed flow rate (kg/s), and dz is the integration step (m).

Temperature Profile

The temperature in the liquid, T (K), obeys the Fourier–Kirchhoff equation, which has the following form in cylindrical coordinates for stationary heat flux (solely vertical liquid flow and negligible axial heat transfer) *(8)*:

$$W_z \frac{\partial T}{\partial z} = \alpha \left(\frac{1}{r}\frac{\partial T}{\partial r} + \frac{\partial^2 T}{\partial T^2} \right) \tag{4}$$

where α is the thermal diffusivity (m^2/s).

The initial and boundary conditions are:

1) $$T = T_0 \text{ for } z = 0 \text{ and } R \le r \le R + S \tag{5}$$

2) $$\frac{\partial T}{\partial r} = 0 \text{ (in the condition of insulated evaporator)} \tag{6}$$

or $$I = I_w \text{ (in the condition of heated evaporator)} \quad \text{for } r = R \text{ and } 0 \le z \le L \tag{7}$$

(3) $$\frac{\partial T}{\partial r} = -\frac{\Sigma\left(E_i \Delta H_i^{vap}\right)}{\lambda} \text{ for } r = R + S \text{ and } 0 \le z \le L \tag{8}$$

where T_w is the temperature on the evaporator surface (K), ΔH_i^{vap} is the evaporation enthalpy (J/kg), and λ is the thermal conductivity (W/mK).

Concentration Profile

The concentration profile, C_i, in the liquid layer for a multicomponent mixture can be expressed by the following equation, which is valid for negligible radial and azimuthal flows and negligible axial diffusion *(8)*:

$$W_z \frac{\partial C_i}{\partial z} = D_i \left(\frac{1}{r} \frac{\partial C_i}{\partial r} + \frac{\partial^2 C_i}{\partial r^2} \right) \tag{9}$$

where D_i is the mass difusivity (m^2/s).

The initial and the boundary conditions are:

(1) $$C_i = C_{i0} \text{ for } z = 0 \text{ and } R \le r \le R + S \tag{10}$$

(2) $$\frac{\partial C_i}{\partial r} = 0 \text{ for } r = R \text{ and } 0 \le z \le L \tag{11}$$

(3) $$\frac{\partial C_i}{\partial r} = - \frac{E_i - C_i M_i \left(\sum_{j=1}^{n} \frac{E_j}{M_j} \right)}{\rho D_i} \text{ for } r = R + S \text{ and } 0 \le z \le L \tag{12}$$

Using condition 3, we can guarantee that the mass balance is completely satisfied.

These equations are modified to a convenient form to apply the finite differences method and solved by an implicit finite differences method *(11)*. The film thickness was divided in 200 equal intervals, and the evaporator length, L, was divided into 100 equal intervals. For each value of z, the value of r will vary from $r = R$ (evaporator wall) to $r = R + S$ (evaporation surface). So, the system of equations is solved in the following way:

1. Solution of equation 1.
2. Solution of equation 3.
3. Solution of equation 2.
4. Solution of the equation system through finite differences generated by equations 4 to 8.
5. Solution of the equation system through finite differences generated by equations 9 to 12.
6. Increase the value of r with Δr.
7. Return to step 4 until $r = R + S$.
8. Increase the value of z with Δz.
9. Return to step 1 until $z = L$.
10. End.

The mathematical method considered is highly stable and the results were convergent after using sufficiently reduced integration step. In this

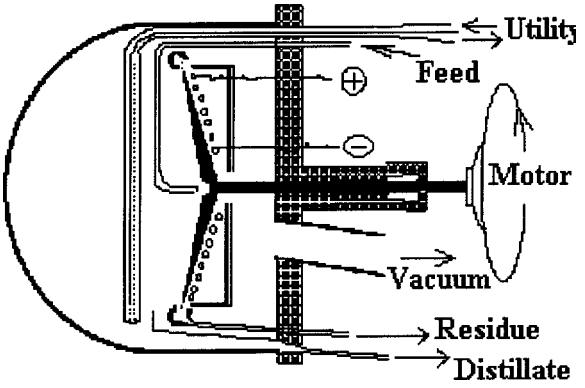

Fig. 3. Centrifugal molecular distillator.

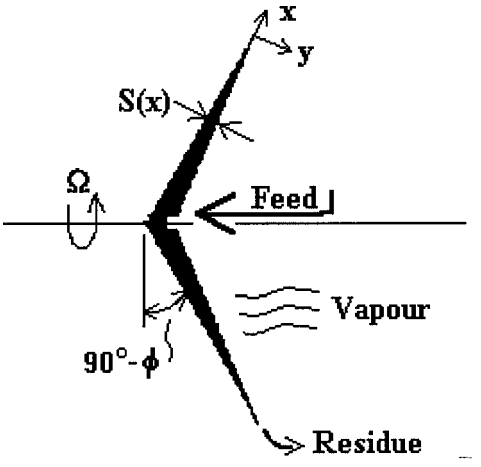

Fig. 4. Coordinate system of the evaporator.

case, Δr was equal to $S/200$ and ΔZ equal to $L/100$. The solution was considered correct after the mass global balance reach values above 99.5%.

Centrifugal Equipment

A typical apparatus for centrifugal molecular distillation is shown in Fig. 3 (conventional scheme shown in the literature). The material fluxes through the apparatus are shown schematically in Fig. 4 *(12)*. The liquid to be distilled is heated until the feed temperature is reached and goes to the evaporator center through pumping. Therefore, the liquid by centrifugal force is uniformly spread on the evaporator until its border is a thin film, where it is partially vaporized, and which vapor is condensed in the condenser.

Surface Evaporation Rate under High Vacuum

In the present analysis, it is assumed that the evaporation rates at the liquid surface are given by the Langmuir equation:

$$E_i = C_{iS} P_i^{\text{sat}} \left(\frac{M_i}{2\pi R_g T_S} \right)^{\frac{1}{2}} \tag{13}$$

where the nomenclatures are analogous to the falling film distillator.

Velocity and Thickness Profiles

The continuity equation for the liquid flowing as a thin film in the coordinate system, as illustrated in Fig. 4, is given by *(12)*

$$\frac{\partial u}{\partial x} + \frac{\partial v}{\partial y} + \frac{u}{x} - \frac{v \cot \phi}{x} = 0 \tag{14}$$

where u and v are the velocity profiles in the directions x and y (axial and diagonal coordinates, respectively) (m/s) and ϕ is the half angle of the evaporator.

The boundary conditions are

$$u = u_0 \text{ at } x = x_0 \text{ (feed)} \tag{15}$$

and

$$v = 0 \text{ at } y = 0 \, . \tag{16}$$

The film thickness $S(X)$(m) is given by

$$S(x) = \left[\frac{\left(m_0 - \sum_{x=x_0}^{x} \left\{ \sum_{i=1}^{n} E_i \right\} \pi \Delta x \sin^2(\phi)(2x + \Delta x) \right)}{\frac{\pi \rho \Omega^2 x \sin^2 \phi}{3\mu} (2x \sin\phi - S\cos\phi)} \right]^{\frac{1}{3}} \tag{17}$$

where μ is the cinematic viscosity (m^2/s), Ω is the angular velocity of the evaporator (rad/s), and n is the total number of components.

Temperature Profile

The energy balance equation gives the temperature profile, T, in the liquid film on the evaporator *(12)*

$$u \frac{\partial T}{\partial x} + v \frac{\partial T}{\partial y} = \alpha \left(\frac{\partial^2 T}{\partial y^2} + \frac{1}{x} \frac{\partial T}{\partial x} - \frac{\cot \phi}{x} \frac{\partial T}{\partial y} \right) \tag{18}$$

with the initial and boundary conditions

$$T = T_0 \text{ at } x = x_0 \text{ (feed)} \tag{19}$$

$$T = T_w \text{ (rotor temperature) at } y = 0 \tag{20}$$

and
$$\frac{\partial T}{\partial r} = -\left[1 + (S')^2\right]^{\frac{1}{2}} \frac{\Sigma\left(E_i \Delta H_i^{vap}\right)}{\lambda} \text{ at } y = S(x) \tag{21}$$

where S′ is written as:
$$S' = \frac{\Delta S}{\Delta x} \tag{22}$$

Concentration Profile

The equation describing the mass transfer in a multicomponent mixture gives the concentration profile in the liquid film, C, and is written as *(12)*

$$u\frac{\partial C_i}{\partial x} + v\frac{\partial C_i}{\partial y} = D_i\left(\frac{\partial^2 C_i}{\partial y^2} + \frac{1}{x}\frac{\partial C_i}{\partial x} - \frac{\cot\phi}{x}\frac{\partial C_i}{\partial y}\right) \tag{23}$$

with the initial and boundary conditions

$$C_i = C_{i0} \text{ at } x = x_0 \tag{24}$$

$$\frac{\partial C_i}{\partial y} = 0 \text{ at } y = 0 \tag{25}$$

and
$$\frac{\partial C_i}{\partial r} = -\left[1 + (S')^2\right]^{\frac{1}{2}} \frac{E_i - C_i M_i\left(\sum_{j=1}^{n} \frac{E_i}{M_j}\right)}{\rho D_i} \text{ at } y = S(x) \tag{26}$$

These equations are modified to the form of finite differences and solved by an implicit finite difference method *(11)*. This method has shown good stability for this application. The film thickness was divided in 200 equal intervals, and the evaporator length, *L*, was divided in 100 equal intervals. For each value of *x*, the value of *y* will vary from $y = 0$ (evaporator wall) to $y = S$ (evaporation surface). Therefore, the system of equations is solved in the following way:

1. Solution of equation 13.
2. Solution of equation 17.
3. Solution of equations 14 to 16.
4. Solution of the equation system through finite differences generated by equations 18 to 22.
5. Solution of the equation system through finite differences generated by equations 23 to 26.
6. Increase the value of *y* with Δy.
7. Return to step 3 until $y = S$.
8. Increase the value of *x* with Δx.
9. Return to step 1 until $x = L$.
10. End.

In this case, also, the implicit finite difference method also was highly stable and the results are convergent after using a sufficiently reduced

integration step. In this case, Δy was equal to $S/200$ and Δx equal to $L/100$. The solution was considered correct after the mass global balance reach values above 99.6%.

Therefore, these equations consider the phenomena of the liquid phase, but do not take into consideration the vapor phase. However, at this point, all conditions at the surface of the liquid film, such as concentration and temperature, where the evaporation phenomena occurs, are defined. Therefore, it is possible, now, to continue with the modeling of the vapor phase. It can be said that the Langmuir equation does not represent the vapor phase realistically on the molecular distillation. A vapor phase modeling has to be considered for this process, as described below.

Vapor Phase Mathematical Modeling

With the conditions at the liquid evaporation surface determined, it is possible to analyze the phenomena that occur in the vapor phase.

The surface evaporation rate on the evaporator for both equipment (falling film and centrifugal) is given by the Langmuir equation, as already mentioned [eq. (1)]:

$$E_i = C_{iS} P_i^{\text{sat}} \left(\frac{M_i}{2\pi R_g T_S} \right)^{\frac{1}{2}} \tag{27}$$

This expression provides exact values of the distillation rate, but only when there is no return of the molecules from the vapor phase to the liquid phase in the evaporator. However, collisions happen in the vapor phase and part of the molecules come back to the evaporator. Thus, studying the molecular dynamics of the vapor phase allows evaluating the amount of molecules that come back to the liquid phase and, consequently, the real deviation of the values given by equation (27). Therefore, the evaporation efficiency is defined as the ratio between the real and the ideal values (this one is given by the Langmuir equation). The smaller the efficiency is, the larger will be the operating time and, therefore, the eventual problems with thermal decomposition of the material. Thus, it is important to determine layouts and operating conditions of the molecular distillation equipment that maximize the evaporation efficiency.

Methodology

The real behavior of the molecules in the vapor phase under high vacuum can be described by the Boltzmann equation *(13)*:

$$u_{zi} \left(\frac{\partial f_i}{\partial z} \right) = \sum_{j=1}^{n} J_{ij} \tag{28}$$

This equation refers to a planar, one-dimensional and steady-state flow, where i represents the species of the vapor mixture, f_i is the distribution function and u_{zi} is the molecular velocity (m/s) in the vapor phase of

component i in the direction z. The symbol J_{ij} represents the integral of the collision for the interaction between species i and j.

To avoid the complex solution of Boltzmann's equation, Bird *(14)* has applied the direct simulation Monte Carlo method (DSMC) in problems involving the dynamics of rarefied gases. Therefore, the Monte Carlo method was considered for the vapor phase modeling and not Boltzmann's equation, because the modeling requires large flexibility due to the complex geometry of the molecular distillator.

The Direct Simulation Monte Carlo Method

Monte Carlo method allows the direct simulation of molecular motions and of intermolecular collisions over small time intervals in the vapor phase. Molecular motions are modeled deterministically, while the collisions are treated statistically. In this method, the simulation is carried out on a battery of cells, which is obtained, by the division of the path that the molecules will pass between the evaporator and the condenser.

The main variables, involving the simulation for this method, are the time interval for the simulation in the vapor phase, the size of each cell, the evaporation rate, the molecular motions, and the intermolecular collisions.

Time Interval

Molecular motions and intermolecular collisions in the vapor phase are computed in each interval of time *dt*: if the vapor phase is to be simulated precisely, *dt* must be nearly infinitesimal, necessitating a large amount of computer time. It is convenient, then, to choose a finite value of *dt*, however, it should be small enough to avoid introducing excessive distortions of properties. In ref *15* it was noted that the value of *dt* can be determined by equation (29).

To evaporate a molecule, a minimum evaporation area equal to the area of the molecular section is necessary, or $\pi d^2/4$, which, multiplying by the absolute rate equation, gives

$$dt = \left(\frac{E_a \pi d^4}{4}\right)^{-1} \tag{29}$$

where *dt* is the time interval (s), *d* is the molecular diameter (m), and E_a is given by equation:

$$E_a = N_{\text{av}} P^{\text{sat}} \left(\frac{1}{2\pi M_m R_g T_S}\right)^{\frac{1}{2}} \tag{30}$$

where E_a is the absolute rate (molecules/m^2s), N_{av} is the Avogadro's number, M_m is the medium mass of a single molecule (kg), and R_g is the gas constant.

The fact is that, many times, the value determined by equation (29) is high, inducing considerable deviations in the simulation results, mainly in the cells where there is high collision density. Thus, it was assumed that the best *dt* value will be determined when the total number of colliding molecules inside the cell with the largest molecular density (next to the

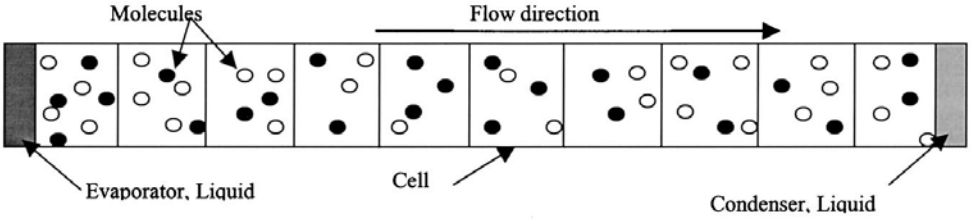

Fig. 5. Computational cells for using in the Monte Carlo simulation.

evaporator) reaches 30–50% of the total number of molecules in this cell. Simulation results showed that the *dt* value calculated in this manner gave results with good precision and reasonable simulation times.

The Size of the Cells

The space between the evaporator and the condenser is divided into cells, according to Fig. 5. In practical terms, the size of a cell must not exceed the value of the mean free path of the molecules for a correct application of the Monte Carlo method. It is known that the largest concentration of molecules occurs near the evaporator. In ref. *16*, it was suggested that the size of the cell should be equal to β/3.

Evaporation Surface Area

The mean free path, β, can be obtained considering a gas in equilibrium:

$$\beta = \frac{R_g T_S}{2^{1/2}\pi d^2 N_{av} P} \tag{31}$$

where P is the system pressure (Pa).

It is necessary now to determine the area (plane perpendicular to the flow of the molecules) of this cell. In practical terms, there are 100–200 molecules for this cell, so that the simulation is not too slow *(14)*.

For the calculation of this area, it was considered the cell nearest to the evaporator. Starting from the expression of E_a (absolute rate, molecule/m2s) and from the time interval dt, the areas (and therefore the volumes, once the axial dimension is known) of the cells containing 100–200 molecules can be determined. If the total area of the evaporator is different from the total area of the condenser, a correction factor should be introduced in the volume for the areas of the subsequent cells until the last cell.

Kinetics of the Molecules (Vapor Phase)

The molecules leave the evaporator (or condenser) and present the following velocity components (17):

Velocity (m/s) in the axial direction of the flow:

$$u = \left(\frac{2kT \ln U_1}{M_m}\right)^{\frac{1}{2}} \tag{32}$$

Velocities (m/s) in the diagonal directions of the flow:

$$v = B\cos(\phi) \tag{33}$$

and

$$w = B\sin(\phi) \tag{34}$$

where

$$B = \left(\frac{2kT_S \ln U_2}{M_m}\right)^{\frac{1}{2}}; \quad \phi = 2\pi U_3$$

k = Boltzman constant and M_m = mass of a single molecule (kg).

These equations are applied for each molecule that evaporates, and they depend on random numbers U_1, U_2, and U_3 uniformly distributed in the interval (0,1). These equations derive from the Maxwel's equations and present a normal distribution for the velocity.

It is also necessary to determine the new velocities of the molecules after the collisions. In ref. *18* collisions were considered hard-sphere, where any direction can be taken by the molecules after the collisions. Thus, this isotropic condition can be used to determine the vectorial velocities of the molecules 1 and 2 (both with same weight) after the collisions. These values (u_1' and u_2') are shown in ref. *4*. Therefore, considering a value of time dt, it is possible to determine the displacement and the new position of each molecule in the vapor space. It is also possible to know the destination of each molecule, in addition to knowing when it reaches the condenser or it comes back to the evaporator. If two molecules collide, the velocity vectors are substituted according to the above equations. If collisions do not occur, the molecules' velocities remain unchanged.

Collisions

Applying the Monte Carlo method for rarefied vapor flow in case of hard-sphere collisions, we have *(4)*:

$$N_c = \frac{N_m}{2}\left(\pi d^2 ng\right)d \tag{35}$$

where N_c is the number of collisions in the cell, n is the number of molecules in the cell, N_m is the number of molecules inside a cell, and g is the average relative velocity (m/s). Then, for each interval of time dt, the total of collisions in a cell will be accepted until to sum N_c collisions. The collision partners are chosen randomly.

Sampling

The macroscopic properties of the vapor phase, as temperature, pressure, and mean free path are calculated through the molecular velocity, are as presented in ref. *4*.

Monte Carlo Method (Vapor Phase)

The simulation of the vapor phase occurring in an interval of time dt, follows:

1. Molecular vaporization on the evaporator inside the closest cell, given by Langmuir's equation (equation 27) in the time interval *dt* (equation 29).
2. Molecular vaporization on the condenser inside the closest cell, also using Langmuir's equation and the consideration of item 1.
3. Determining molecular velocities of the evaporating molecules through equations 32, 33, and 34.
4. Intermolecular collisions occur inside each cell until they reach a value given by equation 35. The molecules that collide acquire new velocity vectors given by equations u', v' and w'.
5. Displacement of the molecules for a time *dt* according to the their velocity vectors.
6. Evaluation of each molecule, in function of its new position (new cell, evaporator or condenser surfaces).

The calculations are carried out sequentially in each cell, and when a cycle (battery of cells) is completed, the total time of simulation is increased by *dt*. This process is repeated until the time that the simulation reaches a preestablished value or a certain variable reaches the steady state (distillation rate, concentration, separation selectivity, etc). The distillation rate is given by the number of molecules that definitely reach the condenser (go out the last cell, next to the condenser). The ratio between the quantity of a particular molecule (component) and the total of molecules that definitely reach the condenser gives the distillate concentration for this species.

DISMOL Simulator

The simulator DISMOL *(1)* presents the architecture described bellow. For each integration step (Δz -falling film; Δx centrifugal) of the liquid phase modeling, the temperature and concentration conditions in the evaporation surface are obtained (item 2). These variables, being known Langmuir's equation is used to determine the amount of molecules that will vaporize. These molecules will be the start-up for the Monte Carlo method, described for the vapor phase (item 3). Finally, results as the distilled rate, compositions, etc. (inside the integration step carried out in the liquid phase) are obtained. A new integration step is carried out in the liquid phase, and the procedure above is repeated. This process will finish when the integration reaches the end of the evaporator. At this point, a global analysis of the distillate and concentrate rates is made and the final separation is determined.

Simulations for Recovering Tocopherols

When DDSO was used directly in the molecular distillator, it was not possible, *a priori*, to obtain a product with high tocopherol concentrations. The process, then, requires a pretreatment to transform heavier components into components of smaller molecular weights. Several methods for

recovering tocopherols from vegetable oils have been studied. The DDSO can be saponified and acidulated to convert glycerides and sterol esters to free fatty acids and free alcohols. The free fatty acids are esterified with a monohydric alcohol of low molecular weight in the presence of a mineral acid catalyst. The sterols are precipitated and crystallized by the addition of water to the mixture, and the tocopherols are concentrated by removing fatty acid esters by molecular distillation *(19)*.

After the molecular distillation process, two flows are generated: one rich in the most volatile component, such as ethyl esters, and another one rich in glycerides and tocopherols. In this work, this method of concentration is being considered, and the conversion of fatty acids to ethyl esters was considered as being of 95%.

Then, the mixture containing 71% ethyl esters (ethyl–palmitate, oleate, stearate, and linoleate), 5% fatty acids not converted (palmitic, oleic, stearic, linoleic acids), 21% glycerides (tri-, di- and monoglycerides), 3% fitosterols (β-sitosterol, stigmasterol) was considered for the modeling and simulation of the falling film and centrifugal molecular distillators. Simulations for the falling film molecular distillator were carried out at different operating temperatures (from 150 to 170°C) and feed flow rate (from 0.3 to 3.0 kg/h) and for simulations of the centrifugal molecular distillator, the operating temperatures (from 180 to 220°C) and the feed flow rate (from 0.3 to 5.0 kg/h) were considered.

Simulations were carried out with variations in the feed flow rate for each operating temperature. The results of the simulations are shown in Figs. 6 and 7. In the process, there are two product streams: the concentrated, rich in tocopherols and in heavier components such as fatty acids, glycerides, and fitosterols, and the distilled, rich in the most volatile component such as ethyl esters and monoglicerides (poor in tocopherols). The presented results refer to the concentrated product stream (Figs. 6 and 7).

Figure 6 shows results of simulations for the falling film molecular distillator for different operating temperatures and feed flow rates. The comparative analyses between the quantity of tocopherol molecules and the total number of molecules that reach the condenser gives the concentration of tocopherols in the distillate flow. It is possible to observe that, for the same temperature, reducing the feed flow rate will increase the tocopherol concentration. This behavior is repeated for all temperatures studied. Moreover, for a fixed feed flow rate, increasing the operating temperature, increases the tocopherol concentration. It can also be verified that the tocopherol concentrations converge to a maximum value, about 38%, in the cases presented.

Figure 7 shows the simulation results for the centrifugal molecular distillator. The same behavior mentioned for the falling film distillator can be observed. However, in this equipment, the concentration converges to values of about 41%, since the operating temperature is higher. The use of temperatures comparatively larger in the centrifugal distillator is due to the fact that this distillation has shorter residence time (on the evaporator)

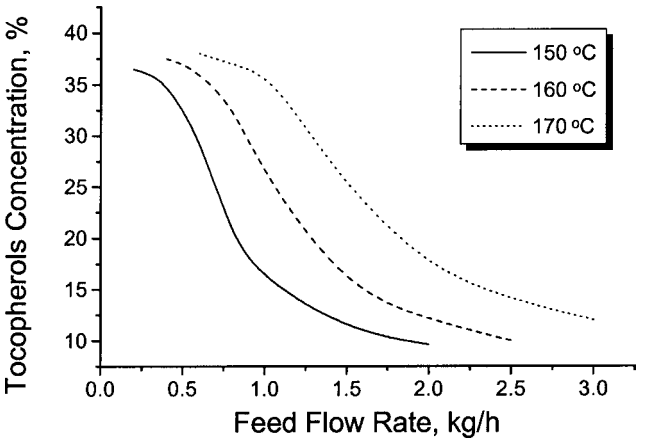

Fig. 6. Tocopherol concentrations in the distillate stream. Falling film distillator.

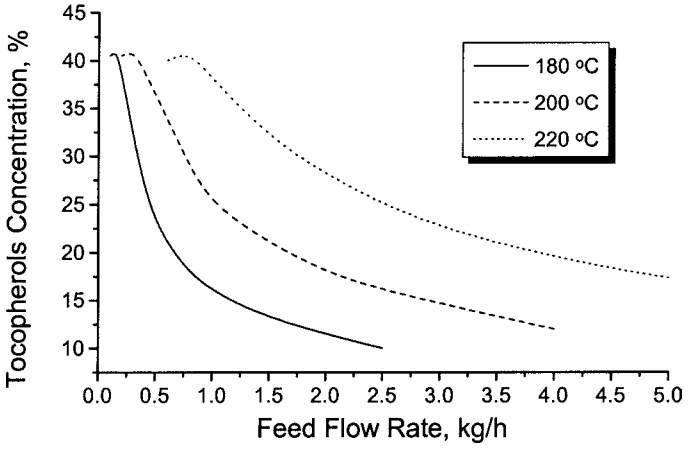

Fig. 7. Tocopherol concentrations in the distillate stream. Centrifugal distillator.

than the falling film distillator, as shown in Figs. 8 and 9. The residence time is determined by the axial velocity equations considering the evaporator length (equation 2 for the falling film and equations 14, 15, and 16 for the centrifugal distillator).

At reduced flows, the residence time, for both equipment, are very long: the residence time of the centrifugal distillator reaches 3.4 s, as is shown in Fig. 8, whereas for the falling film distillator, the residence time is about 370 s (Fig. 9).

Components can be damaged preferentially at high temperatures or at long exposiure times. Products that are damaged when they are exposed for a long time must be handled by the centrifugal distillator, whereas for the products that are more sensitive at high temperatures, the falling film is preferred.

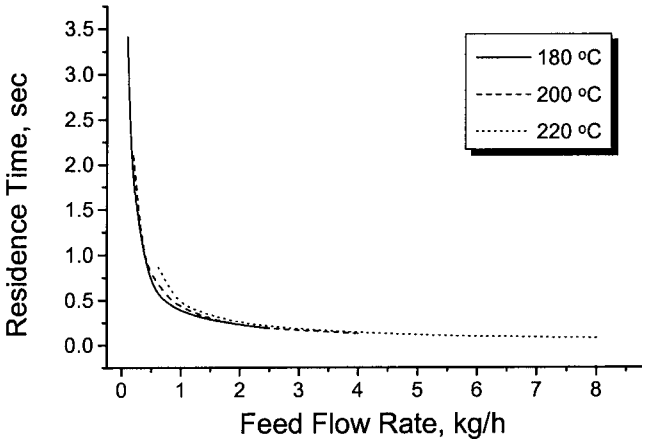

Fig. 8. Residence time vs feed flow rate. Centrifugal distillator.

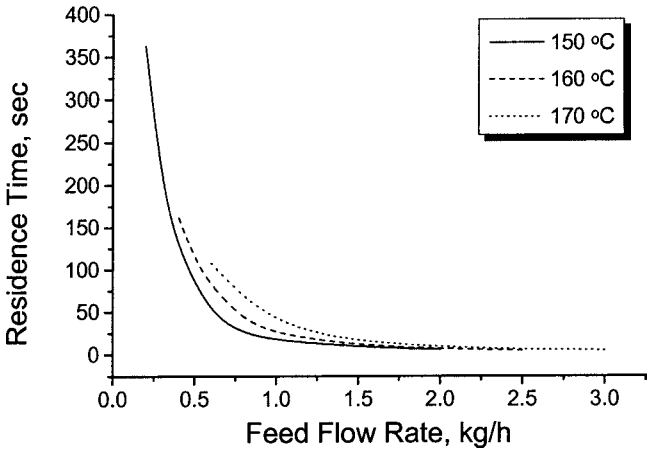

Fig. 9. Residence time vs feed flow rate. Falling film distillator.

Figures 10 and 11 show the residence time profiles under different tocopherol concentrations in both equipment. The higher the concentration is, the longer the contact time of the material on the evaporator will be. Note that for the centrifugal distillator, the residence time is much more sensitive than the falling film at medium tocopherol concentrations for different temperature levels due to higher evaporation rate (high operating temperature) of the centrifugal distillator. This is necessary because the evaporation area is reduced compared to the falling film.

Figures 12 and 13 show the tocopherol concentrations given by equations 9 to 12 for the falling film and 23 to 26 for the centrifugal distillator on evaporation surface in the liquid film: z is the distance for the falling film and x is the distance for the centrifugal distillator. At the beginning, the concentration profile of the centrifugal distillation shows low sensitivity due to the reduced evaporation area near the center of the evaporator;

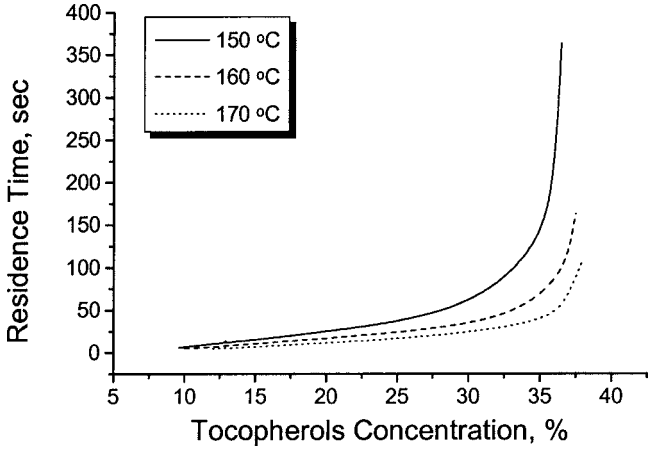

Fig. 10. Residence time vs tocopherol concentration. Falling film distillator.

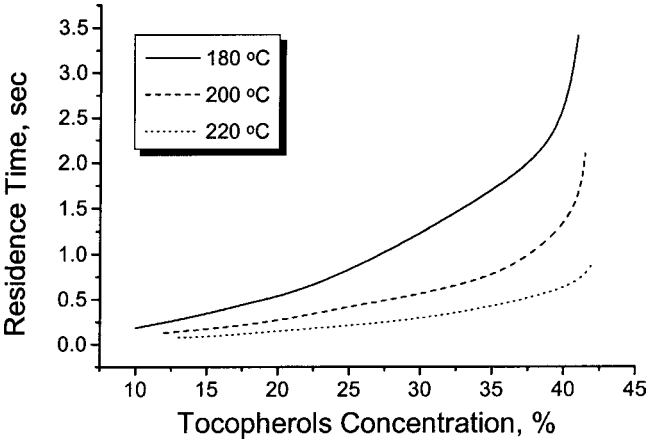

Fig. 11. Residence time vs tocopherol concentration. Centrifugal distillator.

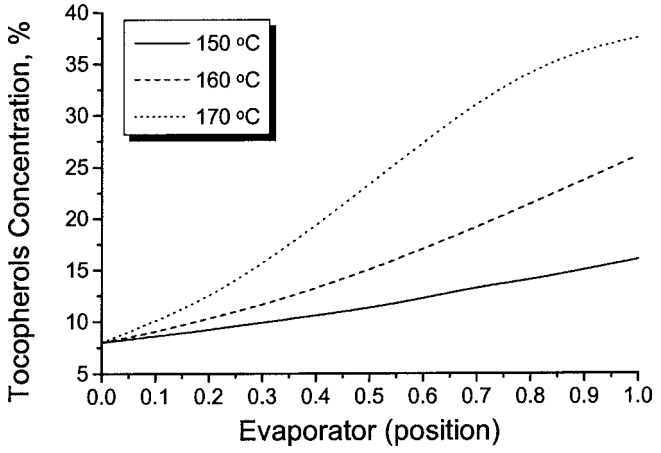

Fig. 12. Tocopherol concentrations in the evaporation surface. Falling film distillator.

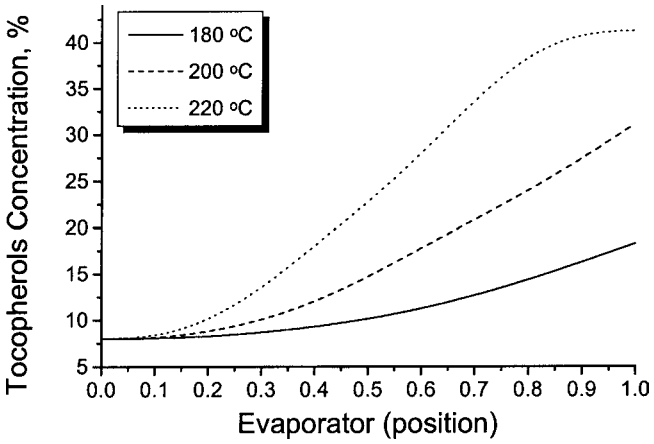

Fig. 13. Tocopherol concentrations in the evaporation surface. Centrifugal distillator.

however, the concentrations acquire similar values to the falling film as the liquid reaches the end of the evaporator.

Concluding Remarks

The use of modeling and simulation applied to the tocopherols recovery one allow to evaluate, *a priori*, the potential of the molecular distillation process for this application. It was possible to obtain concentrations of tocopherol with 40%, starting from a DDSO with 8% of tocopherol, that is, it was possible to concentrate five times the initial material, using just one step of distillation.

Acknowledgments

The authors are grateful to FAPESP (Fundação de Amparo à Pesquisa do Estado de São Paulo) for the financial support for this project (99/04656-9, 99/03550-2, 98/14384-3).

Nomenclature

C Concentration, in mole fraction
C_s Surface concentration, in mole fraction
d Molecular diameter (m)
D_i Diffusion coefficient (m^2/s)
dt Time interval (s)
E Evaporation rate ($kg/m^2 \cdot s$)
E_a Evaporation rate, ($molecules/m^2 \cdot s$)
F Surface ratio
f_i Distribution function
g Gravitational acceleration (m/s^2), molecular relative velocity in the vapor phase (m/s)

h Distance between evaporator and condenser surfaces (m)
J_{ij} Integral of the collision
k Anisotropy of vapor (equation 1), Boltzman constant (vapor phase)
L Evaporator length (m)
m Mass flow rate (kg/s)
M_i Molar mass (kg/kg·mol)
M_m Molecular mass (kg)
n Number of components in the liquid mixture, number of molecules (vapor phase)
N_{av} Avogadro´s number
N_c Number of collisions
N_m Number of molecules
P System pressure (Pa)
P_i^{sat} Vapor pressure (Pa)
r Radial coordinate (m)
R Outer radius of condenser (m)
R_g Universal gas constant, (J/kmol·K)
S Film thickness (m)
T Temperature (K)
T_s Surface temperature (K)
u Velocity in x direction, liquid film or molecules (vapor phase) (m/s)
v Velocity in y direction, liquid film or molecules (vapor phase) (m/s)
w Velocity of the molecules in z direction (m/s)
W_z Velocity in z (m/s)
x Distance along rotor surface (m)
y Distance perpendicular to rotor surface (m)
z Axial coordinate (m)

Greek Symbols

α Thermal diffusivity (m^2/s)
β Mean path of vapor molecule (m)
ΔH Evaporation enthalpy (J/kg)
ϕ Cone half-angle (rad)
λ Thermal conductivity (W/m(K)
η Viscosity (Pa(s)
μ Cinematic viscosity (m^2/s)
ρ Density (kg/m^3)
Ω Rotor speed (rad/s)

References

1. Batistella, C. B. (1999), PhD thesis, UNICAMP, LDPS Campinas-SP, Brazil.
2. Ooi, C. K., Choo, Y. M., Yap, S. C., Barison, Y., and Ong, A. S. H. (1994), *AOCS Press* **71,** 423–426
3. Seetharamaiah, G. S. and Prabhakar, J. V. (1986), *J. Food Sci.Technol.* **23,** 270–273.
4. Batistella, C. B., Maciel, M. R. W., and Maciel Filho, R. (2000), *Computers Chemical Engineering* **24,** 1309–1315.

5. Batistella, C. B. and Maciel, M .R. W. (1996), *Computers Chemical Engineering* **20 (Suppl.),** S19–S24.
6. Eitenmiller, R. R. (1997), *Food Technology* **51(5),** 78–81.
7. Ramamuuthi, S. and McCurdy, A. R. (1993), *AOCS* **70,** 287–295.
8. Kawala, Z. and Stephan, K. (1989), *Chem. Eng. Tech.* **12,** 406–413.
9. Kawala, Z. (1983), *Kinetik der Oberflachenverdamfung unter den Bedingungen der Molekulardestillation*. Wydawnictwo Politechniki Wroclawskiej, Wroclaw, Poland.
10. Batistella, C. B. (1996), MS thesis, UNICAMP, LDPS Campinas-SP, Brazil.
11. Carnahan, B., Luther, H. A., and Wilkes J. O. (1969), *Applied Numerical Methods*, Wiley, NY, pp. 440–442.
12. Bhandarkar, M. and Ferron, J. R. (1988), *Ind. Eng. Chem. Res.* **27,** 1016–1024.
13. Ferron, J. R. (1986), *Ind. Eng. Ch. Fund.* **25,** 594–602.
14. Bird, G. A. (1970), *Phys. Fluids* **13,** 2676–2681.
15. Bhandarkar, M. and Ferron, J. R. (1991), *Ind. Eng. Chem. Res.* **30,** 998–1007
16. Bird, G. A. (1994), *Molecular Gas Dynamics and the Direct Simulation of Gas Flows*, Clarendon Press Oxford, UK.
17. Lutisan, J. and Cvengros, J. (1995), *Chem. Eng. J.* **56,** 39–50.
18. Bird, G. A. (1976), *Molecular Gas Dynamics*, Clarendon Press, Oxford, UK.
19. Smith, F. (1967), US patent no. 3,335,154.